Reaction pathway of nitric oxide oxidation on nano-sized Pt/SiO$_2$ catalysts for diesel exhaust purification

Zhengxu Chen [a], Dezhou Luo [a], Huangwei Zhang [b,c], Na Zhang [a], Junqi Li [a], Bin Gao [a], Run Qiu [a], Yunxiang Li [a], Zhengzheng Yang [a,*]

[a] *College of Environmental Science and Engineering, China West Normal University, Nanchong 637009, China*
[b] *Department of Mechanical Engineering, National University of Singapore, 9 Engineering Drive 1, 117576, Singapore*
[c] *Advanced Manufacturing and Materials Centre, National University of Singapore, Chongqing Research Institute, Chongqing 401123, China*

ARTICLE INFO

ABSTRACT

Catalytic NO oxidation on the diesel oxidation catalyst is of great significance for the low-temperature abatement of diesel soot and NO$_x$ pollutants. Here, a series of Pt/SiO$_2$ catalysts with different particle sizes (2.78–13.94 nm) were prepared and their effects on NO oxidation activity and reaction pathway were investigated. The results show that the size of platinum nanoparticles is a relevant factor for NO oxidation activity by influencing platinum chemical states during the reaction. Furthermore, NO catalytic oxidation on Pt/SiO$_2$ catalysts are primarily through the bidentate nitrite and bridged nitrate intermediates pathways. Relatively larger platinum nanoparticles (~13.94 nm) will lead to the generation of nitrates between layers that are difficult to decompose and desorb from catalyst surface, and thereby adverse to NO oxidation activity. Thus, this work suggests that the size of Pt nanoparticles do not only influence the catalytic NO oxidation activity, but also the reaction pathway on the catalyst.

1. Introduction

Diesel engines are widely applied in transportation vehicles, especially in heavy duty vehicles due to their high thermal- and economic-efficiency [1,2]. However, emissions of carbon monoxide (CO), soot and nitrogen oxides (NO$_x$) from diesel combustion result in environmental pollution and human health damage [3–5]. Thus, in order to meet the increasingly stringent emission regulations, further reducing the harmful pollutants discharged from diesel vehicles is required [6–9]. At present, the main methods to reduce vehicle exhaust pollutants are the in-engine purification technology and exhaust after-treatment system [10]. However, since the former alone is difficult to meet the increasingly stringent emission standards, a diesel exhaust after-treatment system is in high demand [11–13].

An after-treatment system for diesel engines is generally combined with diesel oxidation catalyst (DOC), diesel particulate filter (DPF) and selective catalytic reduction (SCR) catalyst [14–16]. The catalytic conversion of NO to nitrogen dioxide (NO$_2$) on the DOC catalyst is of great significance for decreasing the diesel low-temperature emission of soot particles and NO$_x$ [17–19]. It is well known that NO cannot directly oxidize diesel soot [20]. However, after catalytically oxidizing NO to NO$_2$, the oxidation and abatement of soot particles can therefore proceed according to the C—NO$_2$ and/or C—O$_2$—NO$_2$ reaction routes. It can occur at about 300 °C, which is much lower than the C—O$_2$ route (the major reaction temperature is much higher than 450 °C) [20–23]. On the other hand, catalytic oxidation of diesel exhaust of NO to NO$_2$ is beneficial to the low-temperature SCR performance [24]. Especially, the increased NO$_2$ concentration on the SCR catalyst with NO$_2$: NO = 1: 1 is beneficial to the fast SCR reaction (2NH$_3$ + NO + NO$_2$ → 2N$_2$ + 3H$_2$O) [25–28]. In fact, the fast SCR reaction can eliminate more than 90% of NOx at approximately 250 °C, thereby significantly reducing diesel NO$_x$ low-temperature emissions [25,26].

Platinum (Pt) - supported DOC catalyst is a popular choice for the catalytic oxidation of diesel exhaust NO due to its excellent performance and industrial application prospect [29–31]. The size of Pt nanoparticles on the DOC catalyst plays a key role in the diesel exhaust NO catalytic oxidation reactions [32–34]. It is generally accepted that metallic Pt (Pt^0) is the active component for NO catalytic oxidation, and relatively large Pt nanoparticles can better maintain the Pt^0 state in the preparation and catalytic reaction process. Therefore, the catalyst with relative

* Corresponding author.
E-mail address: zyang@cwnu.edu.cn (Z. Yang).

larger Pt nanoparticle has better NO catalytic oxidation activity [35–37]. The recent model calculation and experimental results indicate that the formation and reduction of $Pt^{\delta+}$ (Pt^{2+} and Pt^{4+}) during the reaction is also an important factor for DOC catalytic activity [38–40]. Our previous works suggested that the DOC catalyst with relative smaller Pt nanoparticle has better NO catalytic oxidation performance under simulative diesel exhaust conditions, due to the smaller Pt nanoparticle is more favourable to regenerate Pt^0 active sites during the long-term use under simulative diesel exhaust conditions [41–43]. However, studies on the effects of nano-sized Pt particle and reaction environment on Pt chemical state and catalytic activity of the Pt-supported DOC catalysts are still scarce.

Especially, to the best of our knowledge, there is little information available in the literature about the effects of Pt nanoparticle size on the reaction route of NO oxidation. While uncovering the reaction route of NO to NO_2 on DOC is of importance for the low-temperature diesel emissions reduction. Therefore, nano-size effect of Pt/SiO_2 catalyst on Pt chemical state, NO oxidation activity and especially its reaction pathway was investigated in this study. High-temperature calcination method was used to control the size of Pt particles. Furthermore, to minimize the effect of strong metal-support interaction resulting from different calcination temperatures [44–46], silicon dioxide (SiO_2) is used as the carrier of the Pt-catalyst. The overarching aims of this work are to identify the effects of Pt nanoparticle size on Pt chemical states during reaction process and uncover the reaction routes of NO oxidation over the catalysts with different sizes of Pt nanoparticles.

2. Experimental method

2.1. Catalyst preparation

The commercial SiO_2 support was supplied by the Sichuan Provincial Vehicular Exhaust Gases Abatement Engineering Technology centre (the specific surface area is about 190 m^2/g, contains 90% SiO_2 and 10% Al_2O_3). Pt/SiO_2 catalysts were prepared through impregnation method, and the total loading amount of Pt was 1.0 wt.%. Firstly, the SiO_2 support was calcinated at 800 °C for 3 h in a muffle furnace. Secondly, the calculated amount of the $(EA)_2Pt(OH)_6$ solution was impregnated on the pretreated SiO_2 support. After drying at 80 °C for 12 h, the obtained powder was divided into four parts and then baked for 2 h under the air flows at 500 °C, 600 °C, 700 °C and 800 °C, respectively. Accordingly, the Pt/SiO_2 catalysts were obtained and marked as cat-500, cat-600, cat-700 and cat-800, respectively.

2.2. Catalytic performance test

About 0.45 g catalyst was placed in a catalytic fixed-bed reactor, and then a gas mixture of NO (1000 ppm)-O_2 (10.0 vol.%)-N_2 was introduced with a gas hourly space velocity (GHSV) of 80,000 $mL{\bullet}g^{-1}{\bullet}h^{-1}$. Afterwards, the reaction temperature was raised to 500 °C with a change rate of 10 °C$\bullet min^{-1}$ and the outlet NO and NO_2 were measured by a NOVA PLUS multi-function flue gas analyser (MRU, Germany). The test was repeated until the NO oxidation ratio curves are constant. Thereafter, the abovementioned sample was used at 500 °C for 3 h under a simulative diesel exhaust gases of 1000 ppm NO, 1000 ppm CO, 330 ppm C_3H_6, 8.0 vol.% CO_2, 7.0 vol.% water vapour, 10.0 vol.% O_2 and N_2. After the catalysts were cooled down to room temperature, their activity was repeatedly tested under the abovementioned simulative diesel exhaust gases conditions with a GHSV of 80,000 $mL{\bullet}g^{-1}{\bullet}h^{-1}$ until the NO oxidation ratio curves are constant. Because of NO_2 is the only product in the NO oxidation reactions under the abovementioned conditions, so the selectivity of NO oxidation is not shown in the following work. The NO oxidation ratio is defined by

$$C_{NO-NO_2} = \frac{[NO_2]outlet}{[NO_x]outlet} \times 100\% \tag{1}$$

where $[NO_2]_{outlet}$ and $[NO_x]_{outlet}$ denote the concentration of NO_2 and NO_x at the outlet, respectively.

2.3. Catalyst characterisation

The textual properties of the samples were tested on a QUAD-RASORB *SI* automated surface area & pore size analyser. Before the test, all the samples were degassed at 300 °C for 3 h, and the experiment was carried out at liquid nitrogen temperature. The specific surface area, pore volume and pore size distribution of the sample were calculated by using the Brunauer-Emmett-Teller (BET) and Barret-Joyner-Halenda (BJH) methods, respectively.

The transmission electron microscope (TEM) FEI TALOS F200X was used to observe the nanoscale morphology and structure of the prepared catalysts.

X-ray diffraction (XRD) experiment was performed on a X' Pert PRO diffractometer using Cu Kα radiation (λ = 0.15418 nm) operated at 40 kV and 45 mA. The XRD data were recorded for 2θ values from 10 ° to 90 °. The crystalline phases were identified by comparison with the reference from the International centre for Diffraction Data (ICDD).

The Thermo Scientific K-Alpha with Al Kα radiation was used to collect X-ray photoelectron spectroscopy (XPS) data. The binding energy shifts of the samples were calibrated using C1*s* binding energy (BE 284.8 eV).

The *in-situ* infrared spectroscopy characterisation was performed on a Thermo Scientific Nicolet iS 50 Fourier Transform Infrared (FT-IR) spectrometer, equipped with a liquid nitrogen cooled MCT detector. About 50 mg finely ground sample of mixed catalyst and KBr with a mass ratio of 1:50 was pressed into a transparent sheet, and then placed in the *in-situ* reaction cell. The gas mixture (1000 ppm NO—N_2) was fed to the sample. After the sample absorbed the mixed gas for 2 min, the *in-situ* cell was evacuated to 5.0×10^{-5} h Pa. Then, the O_2 (10.0 vol.%)-N_2 gas was fed to the sample and the spectra were recorded with a scanning range of 600–4000 cm^{-1}. The background spectra of all samples were recorded under vacuum at 40 °C.

3. Results and discussion

3.1. Catalytic activity

Fig. 1 shows the NO catalytic oxidation performance over all the prepared catalysts. It is generally shown that, the NO oxidation rate first increases as the reaction temperature increases. However, with further increased reaction temperature, the NO oxidation efficiency obviously decreases due to the thermodynamic limitations [47]. For all the samples, the first/second/third test under NO (1000 ppm)-O_2 (10.0 vol. %)-N_2 conditions were marked with the suffix of -cycle1/-cycle2/-cycle3. After performing the abovementioned test cycles, the samples were pretreated and tested under the simulative diesel exhaust gases conditions, and the first/second test under the simulative diesel exhaust gases conditions were marked with the suffix of (DE. 3 h rea.)-cycle1/(DE. 3 h rea.)-cycle2.

As shown in Fig. 1(a), the cat-500 catalyst shows a maximum NO oxidation ratio of approximately 35% at 375 °C in NO (1000 ppm)-O_2 (10.0 vol.%)-N_2 conditions from the first catalytic NO oxidation cycle. In the second cycle, the NO catalytic oxidation performance of the cat-500-cycle2 is significantly increased. This corresponds to a maximum NO oxidation ratio of approximately 55% at 330 °C in NO (1000 ppm)-O_2 (10.0 vol.%)-N_2 atmosphere. After the third cycle, the cat-500-cycle3 sample shows the same catalytic performance with the cat-500-cycle2. Furthermore, the cat-500-cycle3 catalyst was used at 500 °C for 3 h under the simulative diesel exhaust gases (containing 1000 ppm NO, 1000 ppm CO, 330 ppm C_3H_6, 8.0 vol.% CO_2, 7.0 vol.% water vapour, 10.0 vol.% O_2 and N_2 balance) and then marked as cat-500 (DE. 3 h rea.) in Fig. 1. One can see that NO catalytic oxidation activity of the cat-500
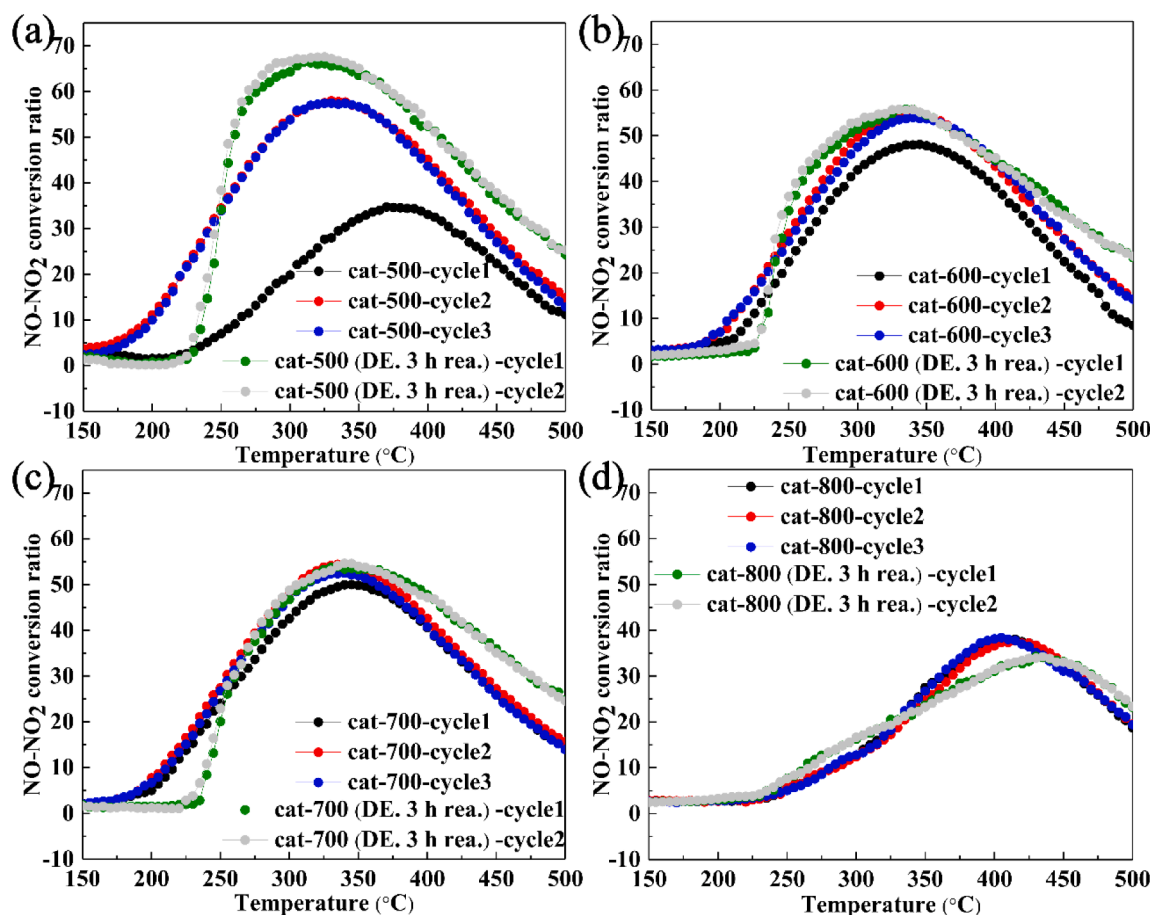
Fig. 1. NO oxidation curves over the catalysts: (a) cat-500, (b) cat-600, (c) cat-700 and (d) cat-800.

(DE. 3 h rea.)-cycle1 further increases, compared to the cat-500-cycle3. Specifically, the maximum NO oxidation ratio of the cat-500 (DE. 3 h rea.)-cycle1 reaches up to 67% at 310 °C under the simulative diesel exhaust conditions. Moreover, the cat-500 (DE. 3 h rea.)-cycle2 shows the same catalytic performance with the cat-500 (DE. 3 h rea.)-cycle1.

Likewise, as shown in Fig. 1(b), the maximum NO oxidation ratio of the fresh cat-600-cycle1 is approximately 49% at 340 °C in NO (1000 ppm)-O_2 (10.0 vol.%)-N_2 conditions in the first cycle. In the second one, the maximum NO oxidation ratio of the cat-600-cycle2 increases up to 55% at 340 °C, and the NO oxidation ratio with the cat-600-cycle3 is the same as that with the cat-600-cycle2. After being used under the simulative diesel exhaust gases at 500 °C for 3 h, the NO oxidation activity of the cat-600 (DE. 3 h rea.)-cycle1 slightly increased. The maximum NO oxidation ratio of the cat-600 (DE. 3 h rea.)-cycle1 is approximately 57% at 330 °C under the simulative exhaust gases, and the cat-600 (DE. 3 h rea.)-cycle2 shows the basically same NO catalytic oxidation activity.

Fig. 1(c) shows the NO oxidation activity of the cat-700 catalyst. The maximum NO oxidation ratio of the cat-700-cycle1 is approximately 48% at 350 °C. After repeatedly performing the catalytic NO oxidation cycle, the catalytic activity shows a slight increase. Specifically, the maximum NO oxidation ratio of the cat-700-cycle2 increases up to about 52% at 335 °C, and the cat-700-cycle3 is the same as that with the cat-700-cycle2. After reactions at 500 °C for 3 h under the simulative diesel exhaust gases, the activity is basically same as that with the cat-700-cycle2 and cat-700-cycle3. The maximum NO oxidation ratio of both the cat-700 (DE. 3 h rea.)-cycle1 and cat-700 (DE. 3 h rea.)-cycle2 are close, approximately 54% at 335 °C under the simulative exhaust gases.

As plotted in Fig. 1(d), the cat-800 shows a significantly lower NO oxidation activity, the maximum NO oxidation ratio of the cat-800 is just approximately 38% at 410 °C in NO (1000 ppm)-O_2 (10.0 vol.%)-N_2

conditions. The catalytic activity of the cat-800 is not increased by the repeated catalytic NO oxidation cycles and long-time use under the simulative diesel exhaust conditions.

To further evaluate the catalytic activity of the above samples, reaction rate and turnover frequency (TOF) have been calculated and summarized in Table 1. Reaction rate was calculated by the equation:

Table 1
NO catalytic oxidation performance over the fresh and aged cat-500, cat-600, cat-700 and cat-800 catalysts.

Samples	T_P (°C)	NO conv. (%)	Rate × 10^{-4} (mol•g^{-1}•s^{-1})	Specific rate × 10^{-6} (mol•m^{-2}•s^{-1})	TOF (s^{-1})
cat-500	375	35	1.46	0.83	0.39
cat-500-cycle3	330	55	2.47	1.40	2.50
cat-500 (DE. 3 h rea.)	310	67	3.11	1.77	0.30
cat-600	340	49	2.16	1.21	1.36
cat-600-cycle3	340	54	2.43	1.36	1.89
cat-600 (DE. 3 h rea.)	330	57	2.56	1.44	0.55
cat-700	350	48	2.09	1.22	1.62
cat-700-cycle3	335	52	2.32	1.35	1.88
cat-700 (DE. 3 h rea.)	335	54	2.43	1.41	0.44
cat-800	410	38	1.51	0.92	–
cat-800-cycle3	410	38	1.51	0.92	–
cat-800 (DE. 3 h rea.)	435	34	1.40	0.85	–

T_P is the reaction temperature of maximum NO oxidation ratio; NO conv. is the value of maximum NO oxidation ratio; TOF value is obtained at 230 °C.

$$Rate = \frac{FX}{vW} \tag{2}$$

$$Specific\ rate = \frac{Rate}{Surface\ area} \tag{3}$$

where F is the inlet molar flow rate of NO, X is the fractional conversion of NO at 230 °C, v is the stoichiometric coefficient of the gas and W is the weight of the catalyst. TOF is the number of NO molecules converted per surface Pt atom per second, and the number of surface Pt atoms of the catalyst is calculated from the average Pt particle size (from TEM results) using sphere model [42,48]. A high GHSV (80,000 h^{-1}) and low NO conversion (less than 20%, catalyst bed temperature is 230 °C) were selected to eliminate the heat and mass transfer limitations and achieve the kinetically controlled conditions [49]. One can see that the reaction rate results match well with the NO oxidation ratio curves (Fig. 1), the fresh cat-600 and cat-700 catalysts show an obviously higher NO oxidation activity than the cat-500 and cat-800. Interestingly, during the reaction process of NO catalytic oxidation, the NO oxidation activity of the cat-500, cat-600 and cat-700 catalysts are significantly enhanced. Especially for the cat-500 catalyst, after NO oxidation reaction cycles, the cat-500-cycle3 shows a better NO oxidation activity than the cat-600-cycle3 and cat-700-cycle3 samples. Moreover, after 3 h using under simulative diesel vehicle exhaust conditions, the NO oxidation activity of the cat-500 (DE. 3 h rea.)-cycle1, cat-600 (DE. 3 h rea.)-cycle1 and cat-700 (DE. 3 h rea.)-cycle1 can be further improved, and the cat-500 (DE. 3 h rea.)-cycle1 shows a significantly better NO oxidation activity than the others. The calculated TOF results show a similar NO oxidation activity trend with the NO oxidation curves and reaction rates. While, all the 3 h used catalysts (-(DE. 3 h rea.)) show an obviously lower TOF value of NO oxidation than the fresh and after 3 times of NO oxidation reaction cycles (-cycle3) samples. This is because of the competitive adsorption of water vapour and C_3H_6 on the NO adsorption sites under the simulative diesel vehicle exhaust conditions [37,50]. To further uncover the reasons about the catalytic performance differences, several relative characterisation methods were carried out in the next section. Due to the catalytic activity of the cat-800 is much lower than the cat-500, cat-600 and cat-700 samples, and not increased by the repeated catalytic NO oxidation cycles and/or long-time use under diesel exhaust conditions. It is of slight significance for the practical application to study the characterisation of cat-800, and hence the cat-800 is not investigated in detail in the subsequent characterisation experiments.

3.2. Catalyst characterisation

3.2.1. N_2 adsorption-desorption

Textual properties of the catalyst are intimately related to the catalytic activity. A large specific surface area is conducive to the dispersion of the active component, and appropriate pore volume and pore size distribution are beneficial to gas/heat transfer [51,52]. To determine the texture properties of the catalysts, N_2 adsorption-desorption techniques were employed. The N_2 adsorption-desorption isotherms of the catalysts are shown in the supporting information Fig. S2, and the calculated results are listed in Table 2. Because of the SiO_2 was calcinated at 800 °C for 3 h before used as the catalyst support, for the fresh cat-500, cat-600, cat-700 and cat-800, as listed in Table 2, all the data of BET specific surface area, pore volume and average pore size are close. It indicates

Table 2
Textual properties of the cat-500, cat-600, cat-700 and cat-800 catalysts.

Samples	Surface area($m^2 \bullet g^{-1}$)	Pore volume($cm^3 \bullet g^{-1}$)	Pore size(nm)
cat-500	176	0.89	20.3
cat-600	178	0.97	19.9
cat-700	172	0.95	20.1
cat-800	165	0.86	20.6

that Pt loading on the SiO_2 carrier and the different temperature calcining of the catalysts do not obviously influence the texture features of the catalysts.

3.2.2. Platinum particle size

Pt nanoparticle size is an important factor for catalytic NO oxidation performance. Fig. 2(a1), (b1) and (c1) show the transmission electron microscopy (TEM) images of the synthesized cat-500, cat-600 and cat-700 catalysts, respectively. One can see that Pt particle size increases with calcining temperature. The Pt nanoparticles (NPs) of the cat-500 catalyst seems amorphous, while those of the cat-600 and cat-700 show obviously crystallographic feature.

The Pt particle distributions of the prepared catalysts were counted from more than 100 Pt particles, obtained from different TEM images of the sample (more TEM images are shown in the supporting information Fig. S1), and the results were plotted in Fig. 2(a2), (b2) and (c2). Fig. 2 (a2) shows that the Pt NPs of cat-500 has a narrow distribution with an average size of approximately 2.78 nm. The Pt NPs on the cat-600 (Fig. 2 (b2)) and cat-700 (Fig. 2(c2)) catalysts have a relatively broad distribution with an average size of about 7.64 nm and 13.94 nm, respectively. Based on fast Fourier transform (FFT) analysis, the interplanar distances of Pt NPs of the cat-600 catalyst are 0.22 and 0.19 nm, which match well with the (111) and the (200) planes of the face-centred cubic Pt, respectively. The Pt NPs of cat-700 also shows two different kinds of interplanar distances of 0.22 nm and 0.19 nm indicating Pt (111) and (200) faces are exposed on the cat-700 catalyst. It indicates that with increased calcination temperature, the Pt NPs size of Pt/SiO_2 catalyst is increased and the Pt crystal structure is more complete.

3.2.3. XRD

To further confirm crystal characteristics of the Pt NPs, XRD was employed. As shown in Fig. 3, all the catalysts of cat-500, cat-600 and cat-700 show a distinct diffraction peak at approximately 22.0 ° which is the typical reflection of SiO_2 (ICDD-PDF#29–0085). The XRD characteristic diffraction peaks of Pt of the cat-500 catalyst are not definitely observed. While, the cat-600 and cat-700 exhibit four peaks at approximately 39.8 °, 46.2 °, 67.5 °and 81.3 °, which can be ascribed to the Pt (111), (200), (220) and (311) faces (ICDD-PDF#04–0802), respectively. The Pt peaks of the cat-700 are obviously sharper and stronger than the cat-600. Combined with the results from TEM, it implies that as catalyst calcination temperature increases, the Pt nanoparticles aggregate on catalyst surface, Pt particle size increases and Pt crystallisation is more complete. However, due to the low Pt loading amount (1.0 wt.%) and the limitation of XRD characterisation, the precise structure and chemical states of Pt species cannot be obtained from XRD results. To further study the states of Pt species, XPS was employed.

3.2.4. XPS

The chemical states of Pt of the catalysts play a key role in NO catalytic oxidation activity. Compared with metallic Pt^0, PtO_x has a weaker binding ability to O_2, O and NO, and the dissociation of O_2 on the surface of PtO_x is more difficult, so the Pt^0 is considered as the active phase of NO catalytic oxidation reaction [48,53,54]. XPS was used to characterize the chemical states of Pt of the prepared catalysts, XPS results of the fresh cat-500, cat-600 and cat-700 catalysts are shown in the supporting information Fig. S3. And Fig. 4 shows the changes of Pt chemical states of the catalysts during the different reaction process of catalytic NO oxidation. Due to the NO catalytic oxidation activity of the cat-700 is similar (slightly lower) with the cat-600, Fig. 4 mainly focus on the changes of the cat-500 and cat-600 samples. As can be seen from Fig. 4 (a), the 71.5 eV peak (the characteristic peak of metallic Pt^0 $4f_{7/2}$ intensity of the cat-500 increased after three times of NO catalytic oxidation reaction cycle under $NO—O_2—N_2$ conditions (cat-500-cycle3). Then, the Pt^0 $4f_{7/2}$ peak intensity of the cat-500-cycle3 increased again after 3 h reaction under simulative diesel exhaust conditions (cat-500 (DE. 3 h rea.). While, compared to the cat-500, the
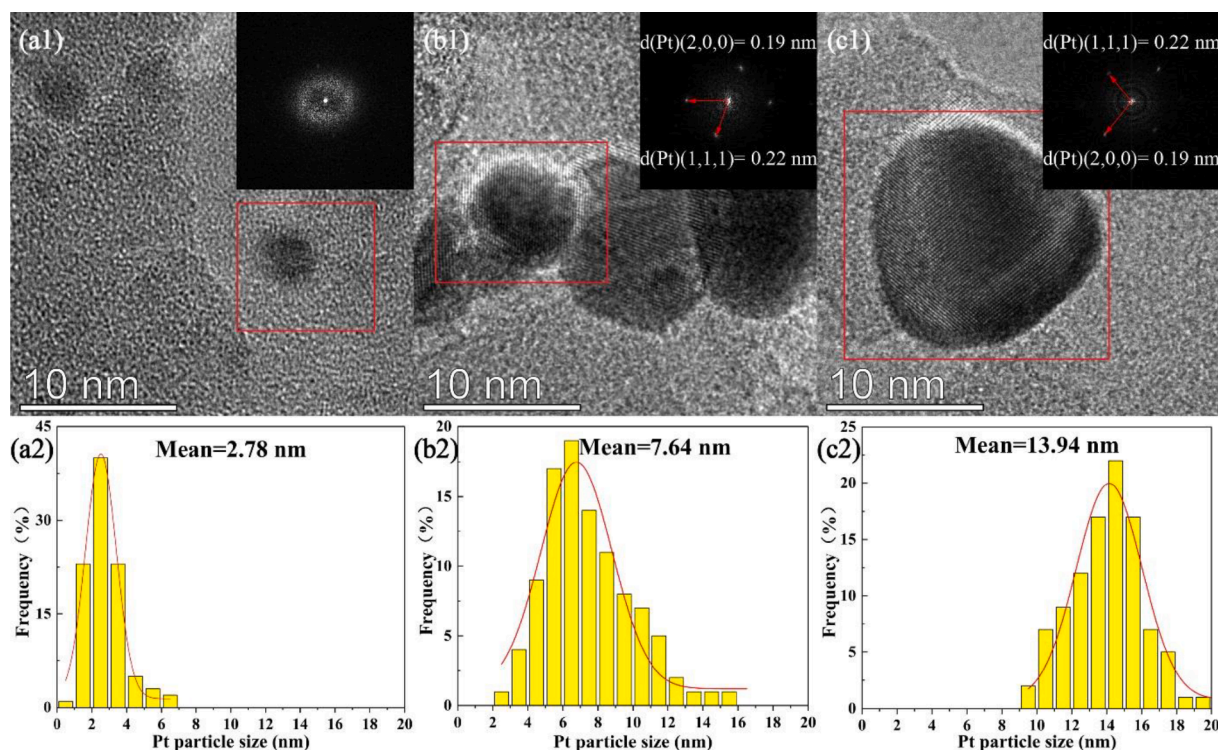
Fig. 2. TEM images (a1–c1) and Pt particle distributions (a2–c2) of the (a1, a2) cat-500, (b1, b2) cat-600 and (c1, c2) cat-700 catalysts.
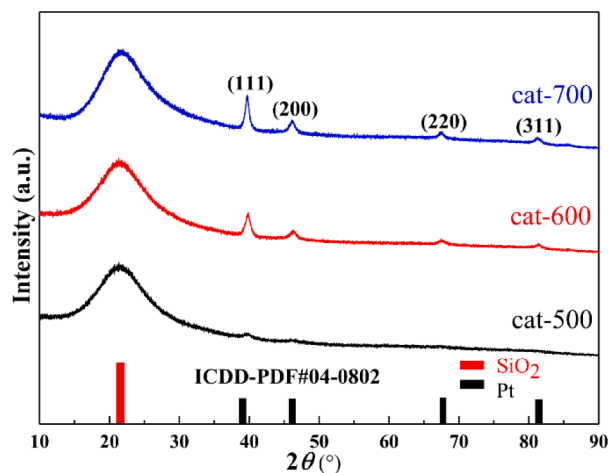
Fig. 3. XRD patterns of the cat-500, cat-600 and cat-700 catalysts.

increasement of Pt^0 $4f_{7/2}$ peak intensity of the cat-600 during the reactions under NO oxidation cycles (NO—O_2—N_2 conditions) and diesel exhaust conditions are relatively lower. It thus can be suggested that the content of metallic Pt^0 over the cat-500 and cat-600 can be increased during the multiple catalytic NO oxidation reaction cycles and/or longtime reaction under diesel exhaust conditions. The cat-500 with smaller Pt nanoparticles (PtO_x) are more easily to be reduced to generate metallic Pt^0 active phase during the NO catalytic oxidation reactions.

Fig. 4(c) and 4(d) show the XPS spectra of Pt $4f$ spectra of the catalysts that were performed by the Fourier transform deconvolution for the quantitative calculation of the Pt species [55,56]. The peak located at 74.4 eV is basically invariable over all the samples which is the Al $2p$ core level spectra. Besides that, all the samples show six peaks at around 71.5, 73.3, 74.8, 74.9, 76.4 and 78.2 eV. The peaks around 74.9 and 78.2 eV are assigned to $4f_{7/2}$ and $4f_{5/2}$ peaks of PtO_2, the peaks around 73.3 and 76.4 eV are assigned to $4f_{7/2}$ and $4f_{5/2}$ peaks of PtO, and the

peaks around 71.5 and 74.8 eV are assigned to $4f_{7/2}$ and $4f_{5/2}$ peaks of metallic Pt^0. Pt species (Pt^0, PtO and PtO_2) ratios are calculated and presented in Table 3. The Pt^0 proportion of the fresh prepared cat-500 is about 35.86% which is remarkably less than that of the cat-600 (about 52.11%). In combination with the results of average Pt particle size of the catalysts from TEM, it indicates that the smaller Pt nanoparticles are more easily to be oxidized to form PtO_x during the preparation process, and the larger Pt nanoparticles can maintain the metallic Pt^0 better during the preparation process. After three times of NO catalytic oxidation reaction cycles, the Pt^0 proportion of the cat-500-cycle3 catalyst is about 62.58%, and that of the cat-600-cycle3 is about 60.69%. This result demonstrates that both the cat-500 with smaller platinum (PtO_x) nanoparticle (~2.87 nm) and the cat-600 with relatively larger platinum (PtO_x) crystalline particle (~7.64 nm) can be reduced by trace of NO to generate Pt^0 species even in oxygen-rich conditions of NO (1000 ppm)-O_2 (10.0 vol.%)-N_2 balance. After 3 h reaction of the abovementioned cat-500-cycle3 and cat-600-cycle3 catalysts under simulative diesel exhaust gases at 500 °C, the $Pt°$ content of the cat-500 (DE. 3 h rea.) is about 81.61% which is markedly more than that of the cat-600 (DE. 3 h rea.) (about 70.73%). Therefore, it can be suggested that after the *in-situ* NO reduction, trace amount of CO and C_3H_6 in the oxygen-rich diesel exhaust gases (1000 ppm NO, 1000 ppm CO, 330 ppm C_3H_6, 8.0 vol.% CO_2, 7.0 vol.% water vapour, 10.0 vol.% O_2 and N_2 balance) can further reduce the PtO_x to Pt^0, and the relatively smaller platinum particles (PtO_x) are more easily to be reduced to form Pt^0 by the diesel exhaust gases. Many studies [35,36,57] have reported that the fresh catalyst with smaller platinum nanoparticles have more PtO/PtO_2 species and with larger platinum particle size generally have more metallic Pt^0, it is mainly because of the smaller ones are much more easily oxidized during the preparation process (generally under air flow). This is actually consistent with the results of this work and our previous works [41,42], the smaller platinum nanoparticles are much more easily oxidized in the preparation process under oxidizing atmosphere (such as air flow), and are also more easily reduced in the presence of reducing gases even under oxygen-rich conditions (such as diesel exhaust, contains trace amounts of NO/CO/C_3H_6
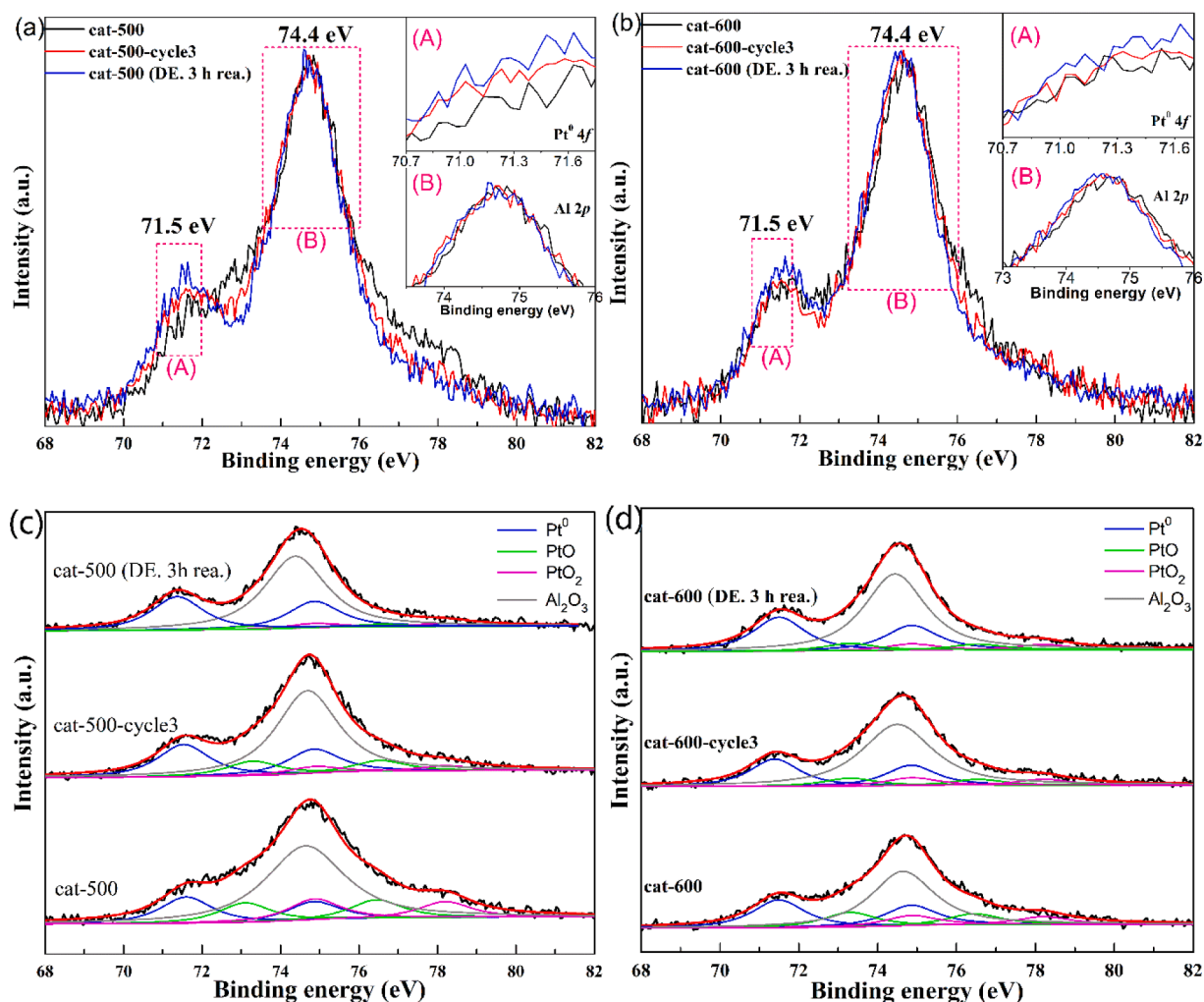
Fig. 4. XPS (Pt 4*f*) spectra of the (a, c) cat-500 and (b, d) cat-600 before and after the catalytic reactions.

Table 3
Pt species ratios from XPS and NO catalytic oxidation performance of the cat-500 and cat-600 before and after the catalytic reactions.

Samples	Pt species ratios (%)			Value of maximum NO oxidation (%)	Reaction temperature of maximum NO oxidation (° C)
	PtO_2	PtO	Pt^0		
cat-500	29.67	34.46	35.86	35	375
cat-500-cycle3	12.77	24.65	62.58	55	330
cat-500 (DE. 3 h rea.)	10.14	8.25	81.61	67	310
cat-600	19.72	28.17	52.11	49	340
cat-600-cycle3	18.49	20.81	60.69	55	340
cat-600 (DE. 3 h rea.)	13.70	15.57	70.73	57	330

and about 10% O_2).

3.3. Reaction pathway of the NO catalytic oxidation

To investigate the catalytic NO oxidation reaction mechanism on the prepared catalysts, the adsorption and chemical conversion of NO and O_2 on the catalysts were studied by *in-situ* FTIR. Fig. 5 presents the *in-situ*

FTIR spectra of the catalyst for NO catalytic oxidation at different reaction temperatures. The cat-500 and cat-600 catalysts have two infrared absorption characteristic peaks at approximately 1235 and 1636 cm^{-1}, which are related to the bidentate nitrite and bridged nitrate, respectively [58–62]. Beside the 1235 and 1636 cm^{-1} peaks, the cat-700 shows an evident absorption peak at approximately 1385 cm^{-1}, which is generally observed in the hydrotalcite materials and assigned to the nitrates between layers [63–66].

In general, for all the prepared catalysts, the peak intensity of the nitrite/nitrate intermediates obviously increased with the increase of reaction temperature from 40 to 275 °C. The peak (1235 and 1636 cm^{-1}) intensity of the cat-500 (Fig. 5a) is significantly lower than that of the cat-600 (Fig. 5b) at the same reaction temperature, in combination with the results of NO catalytic oxidation activity, this is because the nitrite and bridging nitrate intermediates on the cat-500 catalyst can be decomposed to form NO_2 and then desorbed from the catalyst surface more quickly than the cat-600. This is one of the reasons why the cat-500 catalyst has better NO catalytic oxidation activity than the cat-600.

Interestingly, as shown in Fig. 5(c), besides the bidentate nitrite (1235 cm^{-1}) and bridged nitrate (1636 cm^{-1}) intermediates, a new species of nitrates between layers (1385 cm^{-1}) is generated and increased significantly on the cat-700 catalyst. Due to the relatively larger platinum particles of the cat-700, the nitrates can intercalate in the interlayer space between larger platinum particle surface and SiO_2 sheets, as well as the relatively larger platinum interparticles (SiO_2 sheet structure and the interlayer space are shown in Supporting Information
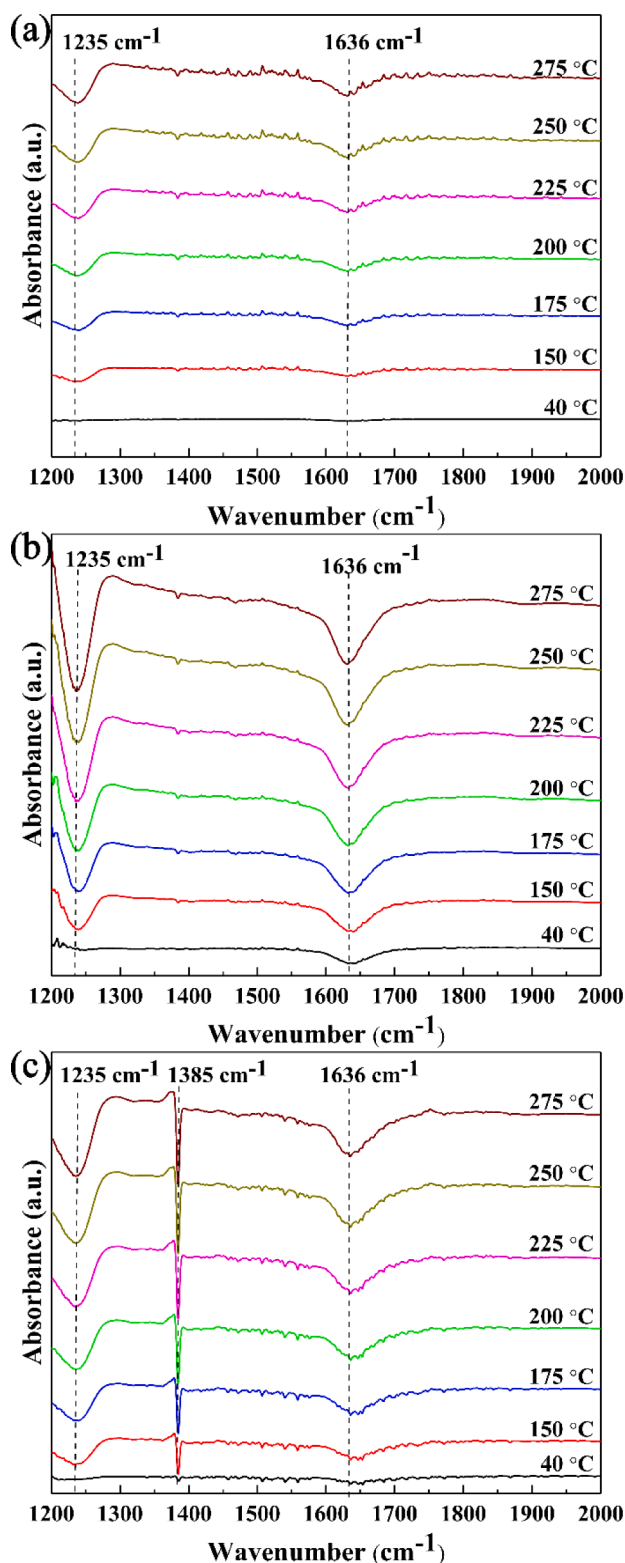
Fig. 5. *In-situ* FTIR spectra of the catalysts under NO/O$_2$ conditions: (a) cat-500, (b) cat-600 and (c) cat-700.

Fig. S4). The nitrates between layers are unperturbed and hard to remove from the catalysts, and therefore close to the active sites [63–65]. It thus can be suggested that the nitrates between layers are relatively difficult to decompose into NO$_x$ species and desorb from catalyst surface, so their accumulation on the catalyst surface will lead to a disadvantage of the catalytic NO oxidation activity of the cat-700

catalyst. It can be seen that the NO catalytic oxidation on Pt/SiO$_2$ catalysts primarily proceeds through the bidentate nitrite and bridged nitrate intermediate pathway. Therefore, smaller Pt nanoparticle size (~2.78 nm) is beneficial for decomposition and desorption of the nitrite/nitrate intermediates, and hence exhibits a superior catalytic NO oxidation activity. Relatively larger Pt nanoparticle size (~13.94 nm) of the catalyst results in production of nitrates between layers, which is difficult to decompose and desorb from catalyst surface, and therefore adverse to the NO catalytic oxidation.

4. Conclusion

The catalytic performance of nano-sized Pt/SiO$_2$ catalysts on oxidizing nitric oxide under diesel exhaust relevant conditions is studied in this work. The results show that Pt nanoparticle size in the Pt/SiO$_2$ catalyst plays a key role on both the catalytic activity and reaction pathway of NO oxidation. For the initial NO catalytic oxidation reaction, the fresh as-synthesized Pt/SiO$_2$ catalysts (cat-600 and cat-700) with relatively larger Pt nanoparticles (7.64–13.94 nm) have better catalytic performance than the cat-500 with smaller Pt particles (~2.78 nm). This is because the larger Pt nanoparticles can maintain more Pt^0 active species during the preparation process. Interestingly, the Pt$^{\delta+}$ species (PtO and PtO$_2$) on the Pt/SiO$_2$ catalysts can be reduced to Pt^0 active species by trace amounts of NO during the NO oxidation reaction cycles, even under the oxygen-rich atmosphere of NO (1000 ppm)-O$_2$ (10.0 vol. %)-N$_2$. The remaining part of Pt$^{\delta+}$ species can be further reduced to form Pt^0 under the simulative diesel exhaust conditions. Moreover, the smaller platinum nanoparticles (PtO$_x$) are more easily to be reduced to form Pt^0 active species under both the NO—O$_2$—N$_2$ and simulative diesel exhaust conditions. Therefore, the cat-500 with smaller platinum nanoparticles (~2.78 nm) shows markedly better NO catalytic oxidation activity than the cat-600 (7.64 nm), cat-700 (13.94 nm) and cat-800 samples after multiple NO oxidation cycles and/or prolonged reaction under simulative diesel exhaust conditions. Besides, NO catalytic oxidation on the Pt/SiO$_2$ catalysts primarily proceeds through the bidentate nitrite and bridged nitrate intermediates pathways. The relatively smaller platinum nanoparticles are beneficial for the decomposition and desorption of the nitrate intermediates and hence improving the catalytic NO oxidation activity. The larger platinum nanoparticles (~13.94 nm) will cause generation of nitrates between layers that are difficult to decompose and desorb from the catalyst surface, and thereby adverse to the NO catalytic oxidation activity.

CRediT authorship contribution statement

Zhengxu Chen: Investigation, Validation, Data curation, Formal analysis, Writing – original draft. **Dezhou Luo:** Validation, Data curation, Formal analysis. **Huangwei Zhang:** Formal analysis, Writing – review & editing. **Na Zhang:** Data curation, Formal analysis, Writing – review & editing. **Junqi Li:** Investigation, Validation. **Bin Gao:** Formal analysis. **Run Qiu:** Formal analysis. **Yunxiang Li:** Formal analysis, Resources, Project administration. **Zhengzheng Yang:** Investigation, Validation, Data curation, Conceptualization, Methodology, Formal analysis, Resources.

Declaration of Competing Interest

The authors declare that they have no known competing financial interests or personal relationships that could have appeared to influence the work reported in this paper.

Acknowledgements

Supplementary materials

Supplementary material associated with this article can be found, in the online version, at doi:10.1016/j.mcat.2021.111991.

References

[1] Q. Liu, C. Bian, S. Ming, L. Guo, S. Zhang, L. Pang, P. Liu, Z. Chen, T. Li, The opportunities and challenges of iron-zeolite as NH_3-SCR catalyst in purification of vehicle exhaust, Appl. Catal. A. Gen. 607 (2020), 117865.

[2] Z. Yang, N. Zhang, H. Xu, Y. Li, L. Ren, Y. Liao, Y. Chen, Boosting diesel soot catalytic combustion via enhancement of solid(catalyst)-solid(soot) contact by tailoring micrometer scaled sheet-type agglomerations of CeO_2-ZrO_2 catalyst, Combust. Flame (2022), https://doi.org/10.1016/j.combustflame.2021.111700.

[3] L. Meng, J. Wang, Z. Sun, J. Zhu, H. Li, J. Wang, M. Shen, Active manganese oxide on MnO_x–CeO_2 catalysts for low-temperature NO oxidation: characterisation and kinetics study, J. Rare Earths 36 (2018) 142–147.

[4] Z. Chen, L. Chen, M. Jiang, X. Gao, M. Huang, Y. Li, L. Ren, Y. Yang, Z. Yang, Controlled synthesis of CeO_2 nanorods and their promotional effect on catalytic activity and aging resistibility for diesel soot oxidation, Appl. Surf. Sci. 510 (2020), 145401.

[5] H.J. Kim, J.H. Lee, M.W. Lee, Y. Seo, J.W. Choung, C.H. Kim, K.Y. Lee, SiO_2@Pd@CeO_2 catalyst with improved thermal stability: effect of interaction between Pd and CeO_2 on activity for CO oxidation, Mol. Catal. 492 (2020), 111014.

[6] N. Zhang, Z. Yang, Z. Chen, Y. Li, Y. Liao, Y. Li, M. Gong, Y. Chen, Synthesis of sulfur-resistant TiO_2-CeO_2 composite and its catalytic performance in the oxidation of a soluble organic fraction from diesel exhaust, Catalysts 8 (2018) 246.

[7] W. Shan, Y. Yu, Y. Zhang, H. He, Advances in the development of exhaust aftertreatment technologies for HeavyDuty diesel vehicles in China, Res. Environ. Sci. 32 (2019) 60–65.

[8] H. Xu, J. Liu, Z. Zhang, S. Liu, Q. Lin, Y. Wang, S. Dai, Y. Chen, Design and synthesis of highly-dispersed WO_3 catalyst with highly effective NH_3–SCR activity for NO_x abatement, ACS Catal. 9 (2019) 11557–11562.

[9] H. Xu, Z. Zhang, J. Liu, C.L. Do-Thanh, H. Chen, S. Xu, Q. Lin, Y. Jiao, J. Wang, Y. Wang, Y. Chen, S. Dai, Entropy-stabilized single-atom Pd catalysts via high-entropy fluorite oxide supports, Nat. Commun. 11 (2020) 3908.

[10] M.J. Kim, E.J. Lee, E. Lee, D.H. Kim, D.-W. Lee, C.H. Kim, K.-Y. Lee, Ag-doped manganese oxide catalyst for gasoline particulate filters: effect of crystal phase on soot oxidation activity, Appl. Surf. Sci. 569 (2021), 151041.

[11] Y. Yang, Z.Z. Yang, H.D. Xu, B.Q. Xu, Y.H. Zhang, M.C. Gong, Y.Q. Chen, Influence of La on CeO_2-ZrO_2 catalyst for oxidation of soluble organic fraction from diesel exhaust, Acta Phys. Chim. Sin. 31 (2015) 2358–2365.

[12] Z. Yang, L. Luo, L. Tang, Z. Zhou, Z. Zhou, Y. Li, Trimesic acid assisted synthesis of cerium-manganese oxide for catalytic diesel soot elimination: enhancement of thermal aging resistibility, Fuel 278 (2020) 118369.

[13] Y. Seo, M.W. Lee, H.J. Kim, J.W. Choung, C. Jung, C.H. Kim, K.Y. Lee, Effect of Ag doping on Pd/Ag-CeO_2 catalysts for CO and C3H6 oxidation, J. Hazard. Mater. 415 (2021), 125373.

[14] Z.Z. Yang, Y. Yang, M. Zhao, M.C. Gong, Y.Q. Chen, Enhanced sulfur resistance of Pt-Pd/CeO_2-ZrO_2-Al_2O_3 commercial diesel oxidation catalyst by SiO_2 surface cladding, Acta Phys. Chim. Sin. 30 (2014) 1187–1193.

[15] Z. Yang, W. Hu, N. Zhang, Y. Li, Y. Liao, Facile synthesis of ceria-zirconia solid solutions with cubic-tetragonal interfaces and their enhanced catalytic performance in diesel soot oxidation, J. Catal. 377 (2019) 98–109.

[16] A. Joshi, Review of vehicle engine efficiency and emissions, SAE Int. J. Adv. Curr. Pract. Mobil. 2 (2020) 2479–2507.

[17] M. Giuseppe, K. Manfred, E. Martin, W. Alexander, The effect of an oxidation precatalyst on the NO_x reduction by ammonia SCR, Ind. Eng. Chem. Res. 41 (2002) 3512–3517.

[18] C. Liu, J.W. Shi, C. Gao, C. Niu, Manganese oxide-based catalysts for low-temperature selective catalytic reduction of NO_x with NH_3 : a review, Appl. Catal. A Gen. 522 (2016) 54–69.

[19] Y. Liang, C. Ou, H. Zhang, X. Ding, M. Zhao, J. Wang, Y. Chen, Advanced insight into the size effect of PtPd nanoparticles on NO oxidation by *in situ* FTIR spectra, Ind. Eng. Chem. Res. 57 (2018) 3887–3897.

[20] N. Zouaoui, M. Labaki, M. Jeguirim, Diesel soot oxidation by nitrogen dioxide, oxygen and water under engine exhaust conditions: kinetics data related to the reaction mechanism, Comptes Rendus Chim. 17 (2014) 672–680.

[21] Y. Li, M. Weinstein, S. Roth, NO oxidation on catalyzed soot filters, Catal. Today 258 (2015) 396–404.

[22] N.D. Wasalathanthri, T.M. SantaMaria, D.A. Kriz, S.L. Dissanayake, C.H. Kuo, S. Biswas, S.L. Suib, Mesoporous manganese oxides for NO_2 assisted catalytic soot oxidation, Appl. Catal. B Environ. 201 (2017) 543–551.

[23] B. Jin, X. Wu, D. Weng, S. Liu, T. Yu, Z. Zhao, Y. Wei, Roles of cobalt and cerium species in three-dimensionally ordered macroporous $Co_xCe_{1-x}O_\delta$ catalysts for the catalytic oxidation of diesel soot, J. Colloid Interface Sci. 532 (2018) 579–587.

[24] S. Zhang, L. Pang, Z. Chen, S. Ming, Y. Dong, Q. Liu, P. Liu, W. Cai, T. Li, Cu/SSZ-13 and Cu/SAPO-34 catalysts for deNO$_x$ in diesel exhaust: current status, challenges, and future perspectives, Appl. Catal. A Gen. 607 (2020), 117855.

[25] R.Q. Long, R.T. Yang, Reaction mechanism of selective catalytic reduction of NO with NH3 over Fe-ZSM-5 catalyst, J. Catal. 207 (2002) 224–231.

[26] X. Shi, F. Liu, L. Xie, W. Shan, H. He, NH_3-SCR performance of fresh and hydrothermally aged Fe-ZSM-5 in standard and fast selective catalytic reduction reactions, Environ. Sci. Technol. 47 (2013) 3293–3298.

[27] H. Zhang, L. Ding, H. Long, J. Li, W. Tan, J. Ji, J. Sun, C. Tang, L. Dong, Influence of CeO_2 loading on structure and catalytic activity for NH_3-SCR over TiO_2-supported CeO_2, J. Rare Earth 38 (2020) 883–890.

[28] C. Sun, W. Chen, X. Jia, A. Liu, F. Gao, S. Feng, L. Dong, Comprehensive understanding of the superior performance of Sm-modified Fe_2O_3 catalysts with regard to NO conversion and H_2O/SO_2 resistance in the NH_3-SCR reaction, Chin. J. Catal. 42 (2021) 417–430.

[29] Y. Ji, T.J. Toops, U.M. Graham, G. Jacobs, M. Crocker, A kinetic and DRIFTS study of supported Pt catalysts for NO oxidation, Catal. Lett. 110 (2006) 29–37.

[30] L. Li, Q. shen, J. Cheng, Z. Hao, Catalytic oxidation of NO over TiO_2 supported platinum clusters. II: mechanism study by *in situ* FTIR spectra, Catal. Today 158 (2010) 361–369.

[31] Z. Hong, Z. Wang, X. Li, Catalytic oxidation of nitric oxide (NO) over different catalysts: an overview, Catal. Sci. Technol. 7 (2017) 3440–3452.

[32] Y. Liang, X. Ding, Z. Du, J. Wang, M. Zhao, Y. Dan, L. Jiang, Y. Chen, Low-temperature performance controlled by hydroxyl value in polyethylene glycol enveloping Pt-based catalyst for CO/C_3H_6/NO oxidation, Mol. Catal. 484 (2020), 110740.

[33] X.P. Auvray, L. Olsson, Sulfur dioxide exposure: a way to improve the oxidation catalyst performance, Ind. Eng. Chem. Res. 52 (2013) 14556–14566.

[34] X. Auvray, T. Pingel, E. Olsson, L. Olsson, The effect gas composition during thermal aging on the dispersion and NO oxidation activity over Pt/Al_2O_3 catalysts, Appl. Catal. B Environ. 129 (2013) 517–527.

[35] L. Olsson, E. Fridell, The influence of Pt oxide formation and Pt dispersion on the reactions NO_2⇔NO+1/2 O_2 over Pt/Al_2O_3 and Pt/BaO/Al_2O_3, J. Catal. 210 (2002) 340–353.

[36] A.D. Smeltz, W.N. Delgass, F.H. Ribeiro, Oxidation of NO with O_2 on Pt(111) and Pt(321) large single crystals, Langmuir 26 (2010) 16578–16588.

[37] X. Auvray, L. Olsson, Stability and activity of Pd-, Pt- and Pd–Pt catalysts supported on alumina for NO oxidation, Appl. Catal. B Environ. 168–169 (2015) 342–352.

[38] A. Arvajová, P. Kočí, V. Schmeißer, M. Weibel, The impact of CO and C_3H_6 pulses on PtOx reduction and NO oxidation in a diesel oxidation catalyst, Appl. Catal. B Environ. 181 (2016) 644–650.

[39] A. Arvajova, P. Koei, Impact of PtOx formation in diesel oxidation catalyst on NO_2 yield during driving cycles, Chem. Eng. Sci. 158 (2017) 181–187.

[40] A. Buzková Arvajová, P. Boutikos, P. Kočí, Differentiation between O_2 and NO_2 impact on PtOx formation in a diesel oxidation catalyst, Chem. Eng. Sci. 195 (2019) 179–184.

[41] Z. Yang, N. Zhang, Y. Cao, M. Gong, M. Zhao, Y. Chen, Effect of yttria in Pt/TiO_2 on sulfur resistance diesel oxidation catalysts: enhancement of low-temperature activity and stability, Catal. Sci. Technol. 4 (2014) 3032–3043.

[42] Z. Yang, J. Li, H. Zhang, Y. Yang, M. Gong, Y. Chen, Size-dependent CO and propylene oxidation activities of platinum nanoparticles on the monolithic Pt/TiO_2-YO$_x$ diesel oxidation catalyst under simulative diesel exhaust conditions, Catal. Sci. Technol. 5 (2015) 2358–2365.

[43] Y.F. Huang, H.L. Zhang, Z.Z. Yang, M. Zhao, M.L. Huang, Y.L. Liang, J.L. Wang, Y.Q. Chen, Effects of CeO_2 addition on improved NO oxidation activities of Pt/SiO_2-Al_2O_3 diesel oxidation catalysts, Acta Phys. Chim. Sin. 33 (2017) 1242–1252.

[44] A.G. Parthasarathi Bera, M.S. Hegde, N.P. Lalla, L. Spadaro, F. Frusteri, F. Arena, Promoting Effect of CeO_2 in combustion synthesized Pt/CeO_2 catalyst for CO oxidation, J. Chem. Phys. 107 (2003) 6122–6130.

[45] J. Wang, X. Dong, Y. Wang, Y. Li, Effect of the calcination temperature on the performance of a $CeMoO_x$ catalyst in the selective catalytic reduction of NO_x with ammonia, Catal. Today 245 (2015) 10–15.

[46] B.F. Pinto, M.A.S. Garcia, J.C.S. Costa, C.V.R. de Moura, W.C. de Abreu, E.M. de Moura, Effect of calcination temperature on the application of molybdenum trioxide acid catalyst: screening of substrates for biodiesel production, Fuel 239 (2019) 290–296.

[47] J. Després, M. Elsener, M. Koebel, O. Kröcher, B. Schnyder, A. Wokaun, Catalytic oxidation of nitrogen monoxide over Pt/SiO_2, Appl. Catal. B Environ. 50 (2004) 73–82.

[48] Z. Yang, N. Zhang, Y. Cao, Y. Li, Y. Liao, Y. Li, M. Gong, Y. Chen, Promotional effect of lanthana on the high-temperature thermal stability of Pt/TiO_2 sulfur-resistant diesel oxidation catalysts, RSC Adv. 7 (2017) 19318–19329.

[49] J. Chen, Y. Wu, W. Hu, P. Qu, X. Liu, R. Yuan, L. Zhong, Y. Chen, Insights into the role of Pt on Pd catalyst stabilized by magnesia-alumina spinel on gama-alumina for lean methane combustion: enhancement of hydrothermal stability, Mol. Catal. 496 (2020), 111185.

[50] L. Olsson, M. Abul-Milh, H. Karlsson, E. Jobson, P. Thormählen, A. Hinz, The effect of a changing lean gas composition on the ability of NO_2 formation and NO_x reduction over supported Pt catalysts, Top. Catal. 30-31 (2004) 85–90.

[51] G. Ziegler, D.P.H. Hasselman, Effect of phase composition and microstructure on the thermal diffusivity of silicon nitride, J. Mater. Sci. 16 (1981) 495–503.

[52] E. Litovsky, M. Shapiro, A. Shavit, Gas pressure and temperature dependences of thermal conductivity of porous ceramic materials: part 2, refractories and ceramics with porosity exceeding 30%, J. Am. Ceram. Soc. 79 (1996) 1366–1376.

[53] O. Louise, P. Hans, F. Erik, S. Magnus, A. Bengt, A kinetic study of NO oxidation and NO_x storage on Pt/Al_2O_3 and Pt/BaO/Al_2O_3, J. Phys. Chem. B 105 (2001) 6895–6906.

[54] K. Hauff, U. Tuttlies, G. Eigenberger, U. Nieken, Platinum oxide formation and reduction during NO oxidation on a diesel oxidation catalyst-experimental results, Appl. Catal. B Environ. 123–124 (2012) 107–116.

[55] M. Hatanaka, N. Takahashi, N. Takahashi, T. Tanabe, Y. Nagai, A. Suda, H. Shinjoh, Reversible changes in the Pt oxidation state and nanostructure on a ceria-based supported Pt, J. Catal. 266 (2009) 182–190.

[56] Q. Yu, M. Richter, F. Kong, L. Li, G. Wu, N. Guan, Selective catalytic reduction of NO by hydrogen over Pt/ZSM-35, Catal. Today 158 (2010) 452–458.

[57] L.M. Carballo, E.E. Wolf, Crystallite size effects during the catalytic oxidation of propylene on Pt/γ-Al$_2$O$_3$, J. Catal. 53 (1978) 366–373.

[58] K. Hadjiivanov, H. Knözinger, Species formed after NO adsorption and NO + O$_2$ co-adsorption on TiO$_2$:an FTIR spectroscopic study, Phys. Chem. Chem. Phys. 2 (2000) 2803–2806.

[59] F. Zhang, S. Zhang, N. Guan, E. Schreier, M. Richter, R. Eckelt, R. Fricke, NO SCR with propane and propene on Co-based alumina catalysts prepared by co-precipitation, Appl. Catal. B Environ. 73 (2007) 209–219.

[60] D. Persson, D. Thierry, N. LeBozec, T. Prosek, *In situ* infrared reflection spectroscopy studies of the initial atmospheric corrosion of Zn–Al–Mg coated steel, Corros. Sci. 72 (2013) 54–63.

[61] L. Qi, Z. Sun, Q. Tang, J. Wang, T. Huang, C. Sun, F. Gao, C. Tang, L. Dong, Getting insight into the effect of CuO on red mud for the selective catalytic reduction of NO by NH$_3$, J. Hazard. Mater. 396 (2020), 122459.

[62] X. Jia, H. Liu, Y. Zhang, W. Chen, Q. Tong, G. Piao, C. Sun, L. Dong, Understanding the high performance of an iron-antimony binary metal oxide catalyst in selective catalytic reduction of nitric oxide with ammonia and its tolerance of water/sulfur dioxide, J. Colloid Interface Sci. 581 (2021) 427–441.

[63] Z.P. Xu, H.C. Zeng, Decomposition pathways of hydrotalcite-like compounds Mg$_{1-x}$Al$_x$(OH)$_2$(NO$_3$)nH$_2$O as a continuous function of nitrate anions, Chem. Mater. 13 (2001) 4564–4572.

[64] A.E. Palomares, J.G. Prato, F. Rey, C. A, Using the "memory effect" of hydrotalcites for improving the catalytic reduction of nitrates in water, J. Catal. 221 (2004) 62–66.

[65] M. Behrens, I. Kasatkin, S. Kühl, G. Weinberg, Phase-pure Cu,Zn,Al hydrotalcite-like materials as precursors for copper rich Cu/ZnO/Al$_2$O$_3$ catalysts, Chem. Mater. 22 (2009) 386–397.

[66] J. Bai, L. Ding, X. Liu, X. Wang, L. Zhang, J. Han, D. Liu, X. Wang, *In-situ* systhesis of CuO/ZnO-Al$_2$O$_3$ catalysts derived from hydrotalcite precursor for catalytic wet air oxidation of phenolic (in Chinese), Acta Sci. Circumst. 38 (2018) 2360–2366.